physiologia

MDPI

Article

Nano-Melittin Attenuates Zearalenone-Induced Ovarian Toxicity by Modulating the Inflammatory–Apoptotic–Steroidogenic Axis in Rats

Rasha Abdeen Refaei [1], Ahmed M. Refaat [2], Amany M. Hamed [3,*], Noha A. R. Fouda [4], Zeyad Elsayed Eldeeb Mohana [5], Rawia M. Ibrahim [6], Ereen Kondos Naeem [7], Gehad S. Mokhtar [8], Pierre E. Mehanny [9], Sherine Nabil Mohammed Fawzy [5], Nagwa M. El-Sawi [3], Elsayed Eldeeb Mehana Hamouda [10] and Nadia S. Mahrous [11]

1 Department of Physiology, Faculty of Medicine, Sohag University, Sohag 82524, Egypt; rasha.abdeen@med.sohag.edu.eg
2 Zoology Department, Faculty of Science, Minia University, Minia 61519, Egypt; ahmed.refaat@mu.edu.eg
3 Chemistry Department, Faculty of Science, Sohag University, Sohag 82524, Egypt; hamde_r2001@yahoo.com
4 Department of Human Anatomy and Embryology, Sohag University, Sohag 82524, Egypt; nohafouda544@yahoo.com
5 College of Medicine, Alexandria University, Alexandria 26571, Egypt; zeyadhamouda@gmail.com (Z.E.E.M.); shery-nabil_97@hotmail.com (S.N.M.F.)
6 Laboratory Diagnosis, Division of Clinical, Department of Animal Medicine, Faculty of Veterinary Medicine, Qena University, Qena 83523, Egypt; r.mounier@vet.svu.edu.eg
7 Department of Pharmacology, Faculty of Veterinary Medicine, South Valley University, Qena 83523, Egypt; ereenkondos@yahoo.com
8 Department of Molecular Biology, Faculty of Applied Biotechnology, Merit University, Sohag 82755, Egypt; gehad.salah@merit.edu.eg
9 Biochemistry, Toxicology and Feed Deficiency Department, Animal Health Research Institute (AHRI), Agriculture Research Center (ARC), Giza 12618, Egypt; pezzat7@gmail.com
10 Department of Pathology, College of Veterinary Medicine, Alexandria University, Alexandria 26571, Egypt; elsayedhamouda@gmail.com
11 Department of Zoology, Faculty of Science, South Valley University, Qena 83523, Egypt; samirnadia89@gmail.com
* Correspondence: amanymohamed@science.sohag.edu.eg

Abstract

Background: Zearalenone (ZEA) is a potent estrogenic mycotoxin that adversely affects the female reproductive system, causing hormonal imbalance, uterine enlargement, structural changes in the reproductive tract, and reduced fertility. This study evaluated the protective effects of melittin-loaded chitosan nanoparticles (MEL-NPs) against ZEA-induced ovarian toxicity in female rats. **Methods**: Forty-eight adult female Wistar rats (180–200 g) were divided into four groups: Control, ZEA, ZEA + MEL, and ZEA + MEL-NPs. ZEA (2.7 mg/kg b.w.) was administered orally twice weekly for two weeks. MEL and MEL-NPs (40 µg/kg b.w.) were given orally three times weekly for one month. Serum biochemical parameters were measured, and ovarian tissues were examined grossly and histopathologically. qRT-PCR was performed to assess mRNA expression of inflammatory markers (TNF-α, IL-6, IL-1β), apoptotic marker (Caspase-3), and steroidogenic enzyme (CYP19A1). **Results**: ZEA exposure induced significant ovarian toxicity, evidenced by increased TNF-α, IL-6, IL-1β, LH, FSH, CA-125, and Caspase-3, along with decreased progesterone, antioxidant capacity, and CYP19A1 expression. Histopathology revealed ovarian atrophy, follicular degeneration, and fibrosis. Treatment with MEL-NPs markedly reversed these alterations, normalizing cytokine and hormonal profiles, restoring CYP19A1 expression, and improving ovarian morphology. MEL-NPs demonstrated superior protective effects compared to free MEL. **Conclusions**: MEL-NPs effectively ameliorate ZEA-induced ovarian toxicity by

Check for updates

Academic Editor: Hiroki Toyoda

Received: 20 February 2026
Revised: 12 March 2026
Accepted: 13 March 2026
Published: 19 March 2026

Copyright: © 2026 by the authors. Licensee MDPI, Basel, Switzerland. This article is an open access article distributed under the terms and conditions of the Creative Commons Attribution (CC BY) license.

restoring hormonal balance, enhancing antioxidant defense, and reducing inflammation and apoptosis. These findings suggest that MEL-NPs could be a promising therapeutic strategy for preventing mycotoxin-induced ovarian dysfunction.

Keywords: zearalenone; ovarian toxicity; melittin nanoparticles; oxidative stress; inflammation; apoptosis

1. Introduction

A non-steroidal mycotoxin with estrogen-like activity, ZEA is sometimes referred to as 6-(10-hydroxy-6-oxo-trans-1-undecenyl)-b-resorcylic acid l-lactone. It belongs to the stable-structured myco-estrogen group of substances. Fusarium species produce it [1,2]. Studies on ZEA have shown that it causes hepato- and hemo-toxicity in addition to immunological toxicity, carcinogenicity, mutagenicity, and genotoxicity [3,4]. Both human and animal reproduction can be impacted by ZEA and its metabolites' ability to bind to estrogen receptors (ERs), behavior by inhibiting ovarian activity (an agonist) [5]. Furthermore, cysts of the ovary, enlarged follicular maturation, an edematous uterus, and ZEA's steroidal qualities may lower the fertilization rate [6].

The primary component of honeybee venom, melittin, has been shown to have numerous biological and pharmacological uses. It possesses inherently antibacterial, antiviral, and anti-inflammatory characteristics [7,8]. It has also been shown to have diverse anti-cancer effects in several cancer cell lines, including those of the gastrointestinal tract. [9,10], breast [7], ovarian [11], and liver origins [12]. Melittin can also stop the cell cycle, preventing cell growth and proliferation [13]. Melittin suppresses the development of ovarian cancer cells by inducing apoptosis through the suppression of signal transducer and activator of transcription 3 (STAT3) and activation of Janus kinase 2 (JAK2), both of which are essential for angiogenesis [14].

Although conventional carriers can typically minimize the number of administration dosages, enhance delivery efficiency, and reduce the side effects of medication toxicity, injectable nanoparticulate carriers offer considerable prospective applications [15,16]. The goal of the research was to create nanoparticles using both synthetic and natural polymers [17]. However, chitosan has garnered considerable attention in the pharmaceutical and medical industries as one of several polymers that create drug-loaded nanoparticles [18]. Chitosan, a biodegradable and biocompatible polymer, is a modified natural carbohydrate and the second most abundant polysaccharide. It can be synthesized by the partial N-deacetylation of chitin, a natural biopolymer derived from crustacean shells such as crabs, shrimps, and lobsters [19,20]. It consists of repeating units of glucosamine and N-acetyl-glucosamine, the proportions of which determine the polymer's deacetylation degree [21]. The ionic gelation process, which produces chitosan nanoparticles by utilizing TPP as a crosslinker, is simple. This method's benefit was attributed to its gentle conditions, which were attained without using toxic organic solvents, heat, or violent agitation that destroys delicate proteins. Additionally, throughout preparation, it may effectively maintain the bioactivity of macromolecules (such as DNA, proteins, etc.) [22].

ZEA has toxic effects that extend beyond hormonal imbalance to include oxidative stress, inflammatory activation, and structural deterioration of ovarian tissue [22]. Recent evidence indicates that zearalenone (ZEA)-induced ovarian toxicity is not limited to estrogen receptor dysregulation but rather involves a tightly interconnected molecular axis linking inflammation, apoptosis, and steroidogenic dysfunction. ZEA exposure has been shown to trigger excessive reactive oxygen species (ROS) generation, leading to activation

of pro-inflammatory signaling pathways and overexpression of key cytokines such as tumor necrosis factor-alpha (TNF-α), interleukin-6 (IL-6), and interleukin-1β (IL-1β), which play pivotal roles in granulosa cell injury and follicular atresia [23]. Sustained inflammatory activation promotes apoptotic signaling through caspase-dependent pathways, particularly caspase-3, a central executioner enzyme associated with granulosa cell loss and diminished ovarian reserve [24]. Concurrently, inflammatory and oxidative insults disrupt ovarian steroidogenesis by suppressing the expression of CYP19A1, the gene encoding aromatase, which is essential for estrogen biosynthesis and normal follicular maturation [25]. Dysregulation of this inflammatory–apoptotic–steroidogenic axis ultimately results in impaired hormonal feedback, ovarian atrophy, and reproductive dysfunction. Therefore, transcriptional profiling of inflammatory mediators, apoptotic markers, and steroidogenic enzymes using quantitative real-time PCR (qRT-PCR) provides a powerful mechanistic tool for elucidating ZEA-induced ovarian injury and evaluating potential protective interventions at the molecular level [26].

The present study investigates a novel therapeutic strategy to mitigate ovarian toxicity induced by zearalenone (ZEA) through the incorporation of melittin into chitosan-based nanoparticles. Although extensive evidence has documented the deleterious effects of ZEA on the female reproductive system, particularly ovarian structure and function, effective protective or therapeutic interventions remain limited. Melittin has shown promising anti-inflammatory and antioxidant properties; however, its clinical applicability is constrained by concerns related to peptide instability and potential cytotoxicity. To overcome these limitations, the current work employs chitosan nanoparticles as a biocompatible and biodegradable delivery system to enhance melittin stability, bioavailability, and functional efficacy. Moreover, this study integrates biochemical, hormonal, histopathological, and molecular assessments, with particular emphasis on qRT-PCR–based analysis of inflammatory, apoptotic, and steroidogenic gene expression. This integrated approach provides mechanistic insight into how nano-formulated melittin modulates the inflammatory–apoptotic–steroidogenic axis to preserve ovarian integrity following zearalenone exposure.

2. Results

2.1. Melittin-Loaded Chitosan–TPP Nanoparticles Characterization

Positively charged chitosan and negatively charged TPP were ionically crosslinked to create the chitosan nanoparticles. Chitosan nanoparticles with melittin were 37.5 nm in size on average. The TEM technique was used to examine the morphological properties of the nanoparticles. The melittin-loaded chitosan nanoparticles have a spherical form and range in size from 26 nm to 49 nm, as shown in Figure 1. The particles are evenly distributed, forming a spherical aggregate of individual particles with distinct connecting boundaries. Chitosan and tripolyphosphate were cross-linked to create melittin-loaded chitosan nanoparticles (TPP). This nano-formulation was centrifuged and collected after the chitosan–TPP nanoparticles were made with melittin attached. A spectrophotometer was then used to quantify the amount of melittin remaining in the supernatant. Melittin-loaded chitosan nanoparticles exhibited a high encapsulation efficiency (EE) of 94.12% and an excellent loading capacity (LC) of 98.77%, indicating highly efficient incorporation of melittin within the nanoparticle matrix. The Fourier-transform infrared (FTIR) spectra of chitosan, melittin, and melittin-loaded nanoparticles (MEL-NPs) are illustrated in Figure 2. The chitosan spectrum (Figure 2A) demonstrated a wide absorption envelope between 3432 and 3286 cm^{-1}, assigned to the overlapping stretching vibrations of hydroxyl (O–H) and amino (N–H) groups, confirming the presence of abundant hydrophilic functional moieties. A clear amide I band appeared at 1641 cm^{-1} due to C=O stretching, accompanied by an amide II band at 1568 cm^{-1} corresponding to N–H bending. Moreover, the signals within

1150–1028 cm^{-1} were attributed to the C–O–C asymmetric stretching of the glycosidic linkages characteristic of chitosan. The melittin spectrum (Figure 2B) displayed intense absorption peaks for N–H stretching vibrations in the range of 3291–2872 cm^{-1}, alongside typical peptide backbone bands including amide I (1646 cm^{-1}) and amide II (1536 cm^{-1}). Additional peaks between 1108 and 465 cm^{-1} reflected C–N and C–C stretching modes associated with the amino acid residues of the peptide. In contrast, the MEL-NPs spectrum (Figure 2C) revealed remarkable spectral modifications. The amide I and amide II bands shifted slightly to 1631 cm^{-1} and 1537 cm^{-1}, respectively, while the O–H/N–H stretching region became broader, extending across 3942–3187 cm^{-1}. Such band shifts and broadening patterns provide strong evidence for electrostatic and hydrogen-bonding interactions between the amino functionalities of chitosan and the peptide groups of melittin. These molecular interactions confirm that melittin was effectively incorporated into the chitosan–TPP polymeric framework, producing a stable nanosystem with successful peptide encapsulation.

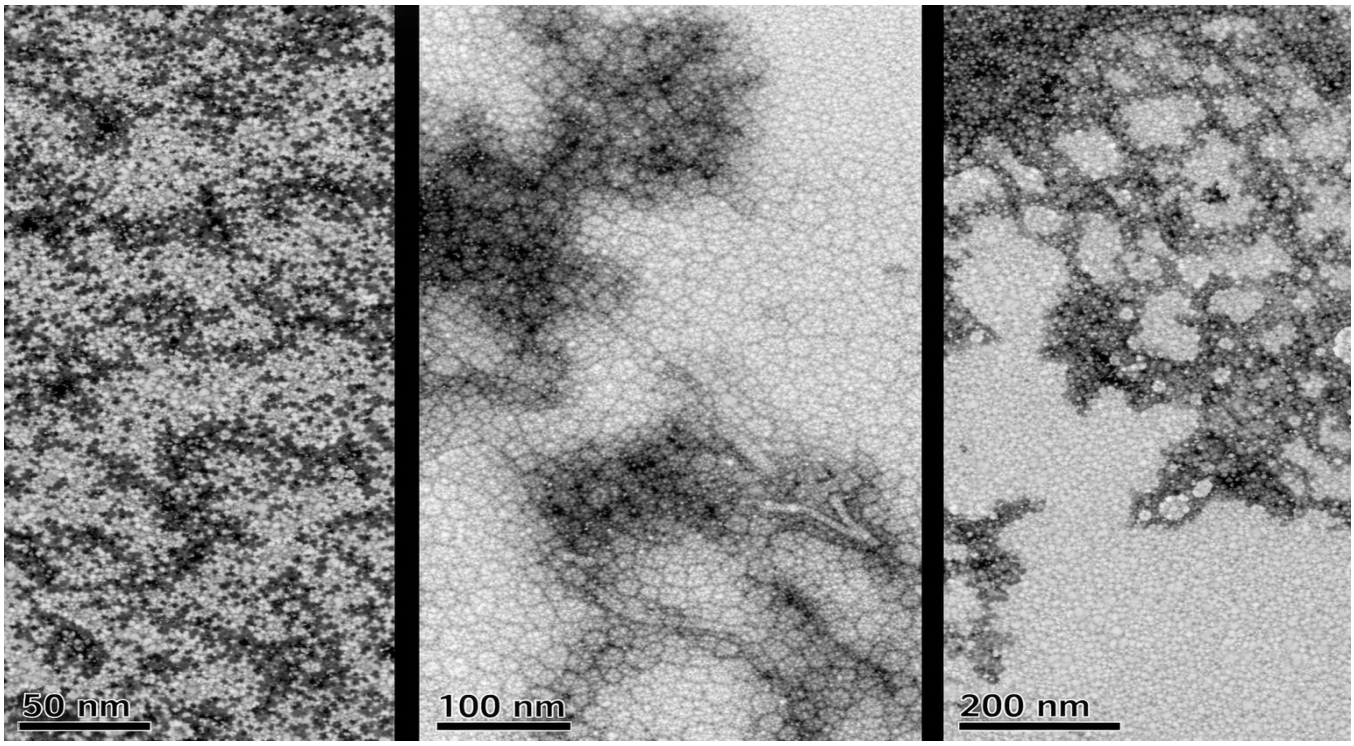


Figure 1. Transmission electron microscopy (TEM) images of melittin-loaded chitosan–TPP nanoparticles (MEL-NPs) at different magnifications. Scale bars represent 50 nm, 100 nm, and 200 nm as indicated. The TEM micrographs reveal that MEL-NPs exhibit a predominantly spherical morphology with a relatively smooth surface and good dispersion, indicating successful nanoparticle formation via the ionotropic gelation method. The average particle diameter was approximately 37.5 ± 2.4 nm, confirming the nanoscale size suitable for efficient cellular uptake and controlled drug release.

2.2. Effect of Zearalenone and Melittin (Free and CS NPs) on Ovarian Inflammatory Markers in Female Rats

As shown in Figure 3, the concentrations of pro-inflammatory cytokines tumor necrosis factor-alpha (TNF-α), interleukin-6 (IL-6), and interleukin-1 beta (IL-1β) were significantly elevated in the ovarian tissues of zearalenone (ZEA)-treated rats compared with the control group, indicating the induction of inflammatory responses. Treatment with melittin (MEL) and melittin-loaded nanoparticles (MEL-NPs) markedly reduced the elevated cytokine levels compared with the ZEA group. The MEL-NP-treated group demonstrated a more

pronounced reduction in TNF-α, IL-6, and IL-1β concentrations than the Free MEL group, suggesting a stronger anti-inflammatory effect of the nanoparticle formulation.

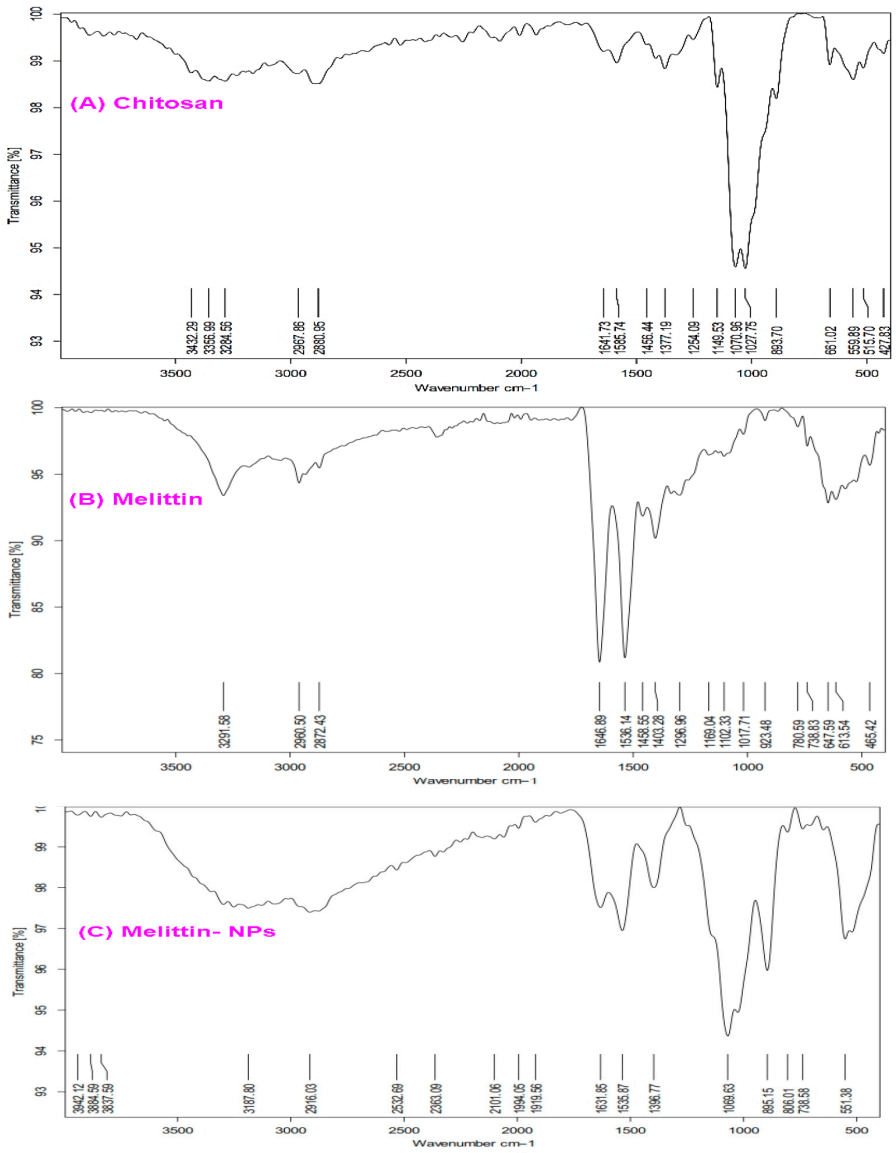


Figure 2. FT-IR spectra of (**A**) chitosan, (**B**) melittin, and (**C**) melittin-loaded chitosan nanoparticles (MEL-NPs). The FT-IR spectra illustrate characteristic functional groups of chitosan and melittin and confirm the successful encapsulation of melittin within the chitosan nanoparticle matrix. In MEL-NPs, notable shifts in the amide I (1647 → 1632 cm^{-1}) and amide II (1536 → 1533 cm^{-1}) bands, as well as the broadening of the O–H/N–H stretching region (3402–3168 cm^{-1}), indicate hydrogen bonding and electrostatic interactions between the amino groups of chitosan and the peptide chains of melittin.

2.3. Effect of Zearalenone and Melittin (Free and CS NPs) on Serum CA-125 and Caspase-3 in Female Rats

As illustrated in Figure 4, rats treated with zearalenone (ZEA) exhibited a significant elevation in the serum levels of CA-125 and caspase-3 compared with the control group, indicating ovarian tissue injury and activation of apoptotic pathways. Administration of melittin (MEL) or melittin-loaded nanoparticles (MEL-NPs) markedly reduced the elevated levels of both CA-125 and caspase-3 compared with the ZEA group. The MEL-NP-treated group showed a more pronounced reduction than the free MEL group, restoring the values toward those of the control.

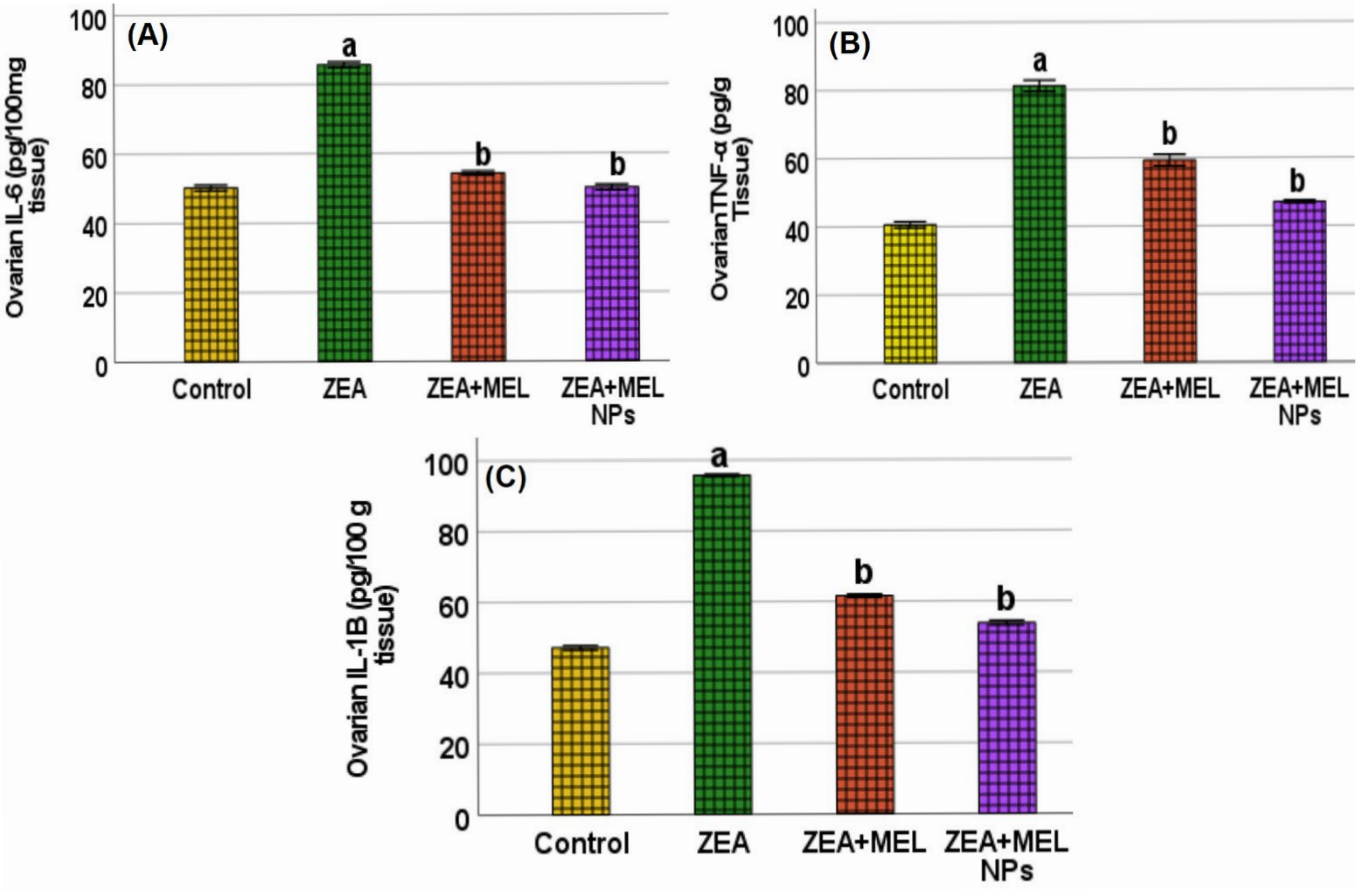


Figure 3. Effect of MEL-NPs treatment on pro-inflammatory cytokines (**A**) IL-6, (**B**) TNF-α, and (**C**) IL-1β in ovarian tissues of rats with ZEA-induced ovarian toxicity. Data are expressed as mean ± S.E.M. (n = 12 rats per group). Statistical analysis was performed using one-way ANOVA followed by Tukey's post hoc test. A p-value < 0.05 was considered statistically significant. [a] $p < 0.001$ vs. control group; [b] $p < 0.001$ vs. ZEA group. IL-6: interleukin-6; IL-1β: interleukin-1β; TNF-α: tumor necrosis factor-alpha; MEL-NPs: melittin-loaded chitosan nanoparticles; ZEA: zearalenone.

2.4. Effect of Zearalenone and Melittin (Free and CS NPs) on Ovarian Tissue Antioxidants in Female Rats

As shown in Figure 4, the total antioxidant capacity in serum was significantly reduced in rats treated with zearalenone (ZEA) compared with the control group, indicating oxidative stress and depletion of endogenous antioxidant defenses. Conversely, treatment of ZEA-exposed rats with melittin (MEL) or melittin-loaded nanoparticles (MEL-NPs) significantly increased the ovarian antioxidant levels compared with the ZEA group. The MEL-NP-treated group exhibited a greater improvement than the Free MEL group, restoring antioxidant capacity close to control values.

2.5. Effect of Zearalenone, Melittin, and Melittin-CS NPs on Ovarian Gene Expression of Inflammatory and Steroidogenic Markers in Female Rats

As shown in Figure 5, the mRNA expression levels of the inflammatory genes TNF-α, IL-6, and IL-1β were markedly upregulated in the ovarian tissues of rats exposed to zearalenone (ZEA) compared with the control group, confirming the activation of inflammatory signaling pathways at the transcriptional level. Additionally, ZEA administration caused a significant increase in the gene expression of the apoptotic marker Caspase-3, indicating enhanced apoptotic activity within the ovarian tissue.

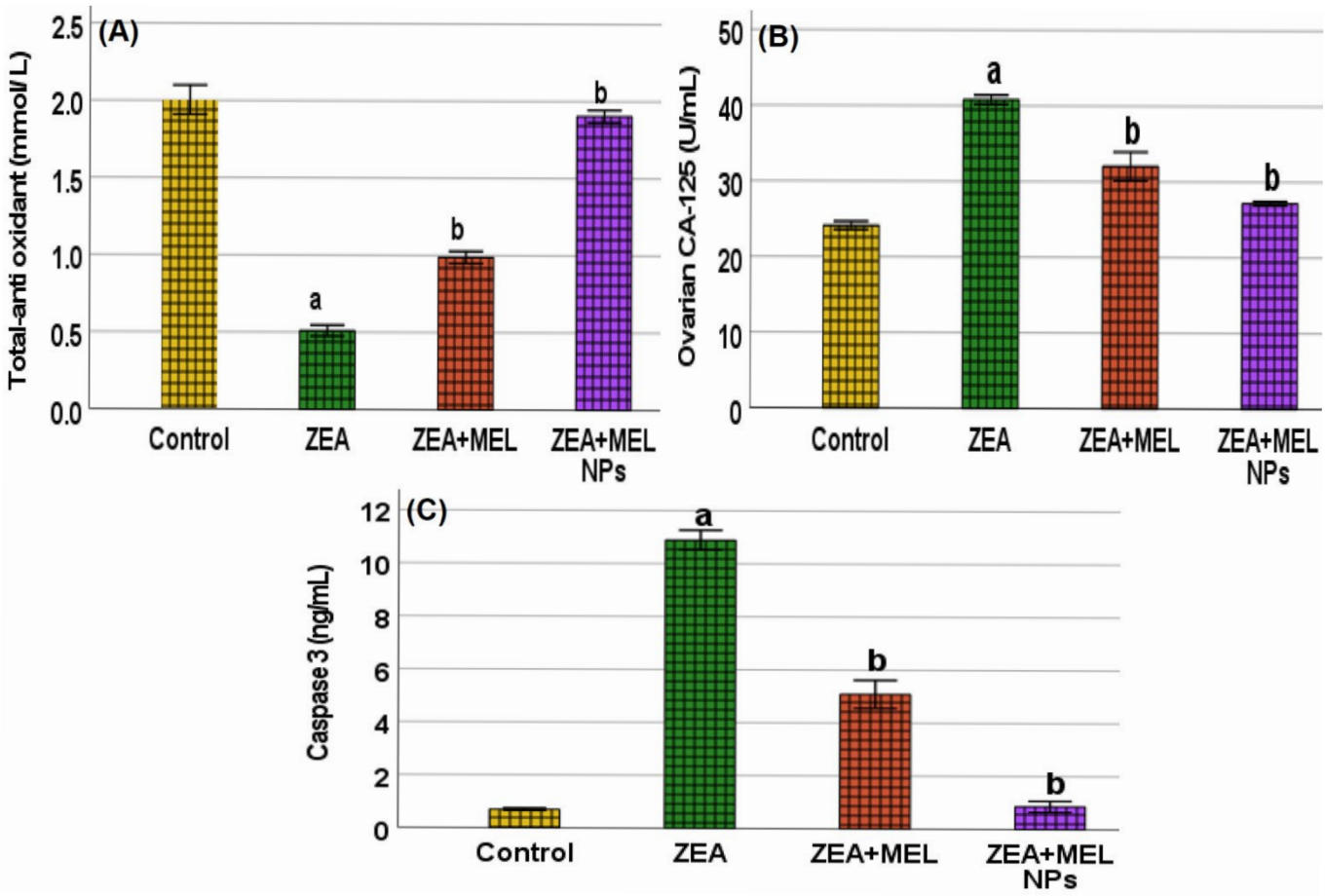


Figure 4. Effects of MEL-NPs therapy on (**A**) antioxidant levels, (**B**) CA-125, and (**C**) Caspase-3 activity in ovarian serum of rats with ZEA-induced ovarian toxicity. Data are expressed as mean ± S.E.M. (n = 12 rats per group). Statistical analysis was performed using one-way ANOVA followed by Tukey's post hoc test. A p-value < 0.05 was considered statistically significant. [a] $p < 0.001$ vs. control group; [b] $p < 0.001$ vs. ZEA group. CA-125: cancer antigen 125; MEL-NPs: melittin-loaded chitosan nanoparticles; ZEA: zearalenone.

In contrast, the expression of the key steroidogenic enzyme CYP19A1 (aromatase) was significantly downregulated in the ZEA-treated rats, reflecting impaired steroidogenic capacity.

Treatment with free melittin (MEL) and melittin-loaded chitosan nanoparticles (MEL-NPs) effectively reversed the ZEA-induced alterations. Both treatments significantly reduced the overexpression of TNF-α, IL-6, IL-1β, and Caspase-3, while simultaneously restoring CYP19A1 expression toward normal levels. Notably, the MEL-NPs group exhibited a more substantial improvement in gene expression than the free MEL group, indicating the superior anti-inflammatory, anti-apoptotic, and steroidogenesis-enhancing effects of the nanoparticle formulation.

2.6. Effect of Zearalenone, Melittin, and Melittin-CS NPs on Ovarian Hormones in Female Rats

As shown in Table 1, the serum levels of FSH and LH were significantly increased in rats treated with zearalenone (ZEA) compared with the control group. Treatment of ZEA-exposed rats with melittin (MEL) or melittin-loaded nanoparticles (MEL-NPs) significantly reduced the elevated FSH and LH concentrations, and the MEL-NP-treated group showed values comparable to the control group.

In contrast, serum progesterone levels were markedly decreased in the ZEA-treated rats compared with the control group, indicating suppression of ovarian steroidogenesis.

Co-treatment with MEL or MEL-NPs significantly increased progesterone levels relative to the ZEA group, with MEL-NPs showing greater improvement than free MEL.

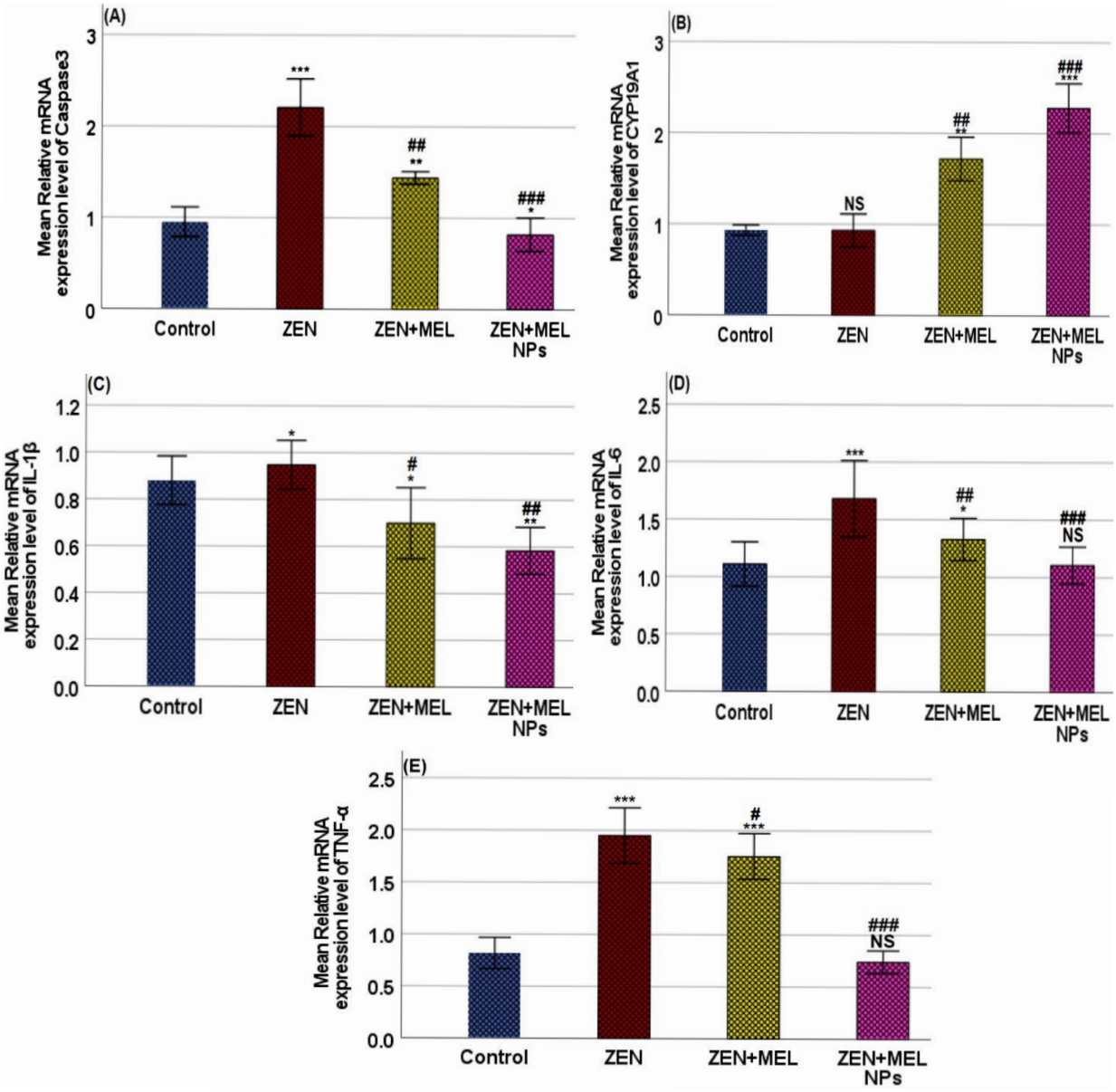


Figure 5. Effect of melittin and melittin nanoparticles on (**A**) caspase-3, (**B**) CYP19A1, (**C**) IL-1β, (**D**) IL-6, (**E**) TNF-α gene expressions in ZEN-induced ovarian toxicity. Expression levels were calculated using the $2^{-\Delta\Delta Ct}$ method following normalization to the housekeeping gene. Data are expressed as mean ± SD (n = 5). Statistical analysis was performed using one-way ANOVA followed by Tukey's post hoc test. *, **, and *** indicate significant differences compared with the control group ($p < 0.05$, $p < 0.01$, and $p < 0.001$, respectively), and NS indicates non-significant differences compared with the control group ($p > 0.05$. #, ##, and ### indicate significant differences compared with the ZEN-treated group ($p < 0.05$, $p < 0.01$, and $p < 0.001$, respectively).

The estradiol (E2) concentration showed no significant differences among the control, ZEA, and treated groups, indicating that the oral administration of ZEA, MEL, or MEL-NPs did not substantially affect serum E2 levels under the current experimental conditions.

Overall, these results indicate that MEL-NPs effectively restored hormonal balance altered by ZEA exposure by normalizing FSH, LH, and progesterone levels toward normal values.

Table 1. Effect of ZEA (2.7 mg/kg B.W.), MEL (40 µg/kg B.W.), and MEL NPs (40 µg/kg B.W.) on serum hormone levels of female rats.

Parameters/Groups	Control	ZEA	ZEA + MEL	ZEA + MEL NPs	*p* Value
FSH (mIU/mL)	1.80 ± 0.09	12.02 ± 0.21 [a]	3.06 ± 0.03 [b]	2.10 ± 0.08 [b]	<0.001
LH (mIU/mL)	1.61 ± 0.12	8.09 ±0.07 [a]	3.30 ± 0.08 [b]	2.44 ± 0.09 [b]	<0.001
E2 (pg/mL)	28.66 ± 1.11	31.42 ±4.421 [NS]	32.58 ± 1.49 [NS]	26.17 ± 0.95 [NS]	0.231
Progesterone(ng/mL)	33.39 ± 0.43	8.99 ± 0.16 [a]	18.87 ± 0.26 [b]	30.75 ± 0.47 [b]	<0.001

Data are presented as mean ± S.E.M. (n = 12 rats per group). Statistical analysis was performed using one-way ANOVA followed by Tukey's post hoc test. A p-value < 0.05 was considered statistically significant. [a] $p < 0.001$ vs. control group; [b] $p < 0.001$ vs. ZEA group; [NS] = $p > 0.05$ (non-significant). FSH: follicle-stimulating hormone; LH: luteinizing hormone; E2: estradiol; MEL: melittin; MEL-NPs: melittin-loaded chitosan nanoparticles; ZEA: zearalenone.

2.7. Morphological Observations of the Uterus and Ovary

As shown in Figure 6, remarkable morphological alterations were observed in the reproductive organs of zearalenone (ZEA)-treated rats. The uterine horns appeared regionally or diffusely dilated and filled with proteinaceous fluid, while the oviducts and ovarian corpora lutea were markedly prominent, congested, and reddish in color in the ZEA group (panel B), compared with the thin and normal appearance observed in the control group (panel A). In contrast, the melittin (MEL)-treated group (panel C) and the melittin-loaded nanoparticle (MEL-NP)-treated group (panel D) exhibited a typical, nearly normal uterine morphology, with the MEL-NP-treated rats showing a more pronounced improvement in structural integrity and reduced congestion compared with the free MEL group.

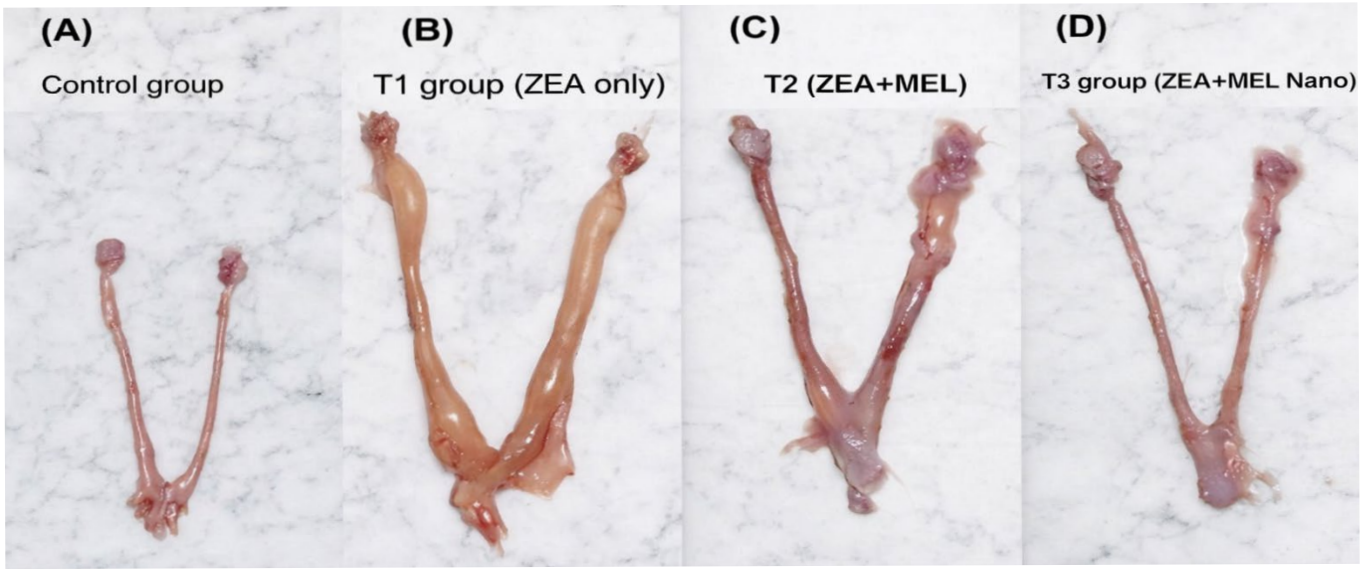


Figure 6. Morphological appearance of the uterus and ovaries in the experimental groups (from the present study). Representative photographs showing macroscopic changes in the uterus and ovaries of female rats from different treatment groups. The ZEA-treated group exhibited regional or diffuse uterine horn distention filled with proteinaceous fluid, along with congested oviducts and prominent reddish corpora lutea, indicating inflammatory reactions. In contrast, rats treated with MEL and MEL-NPs showed a nearly normal appearance of the uterine horns and ovaries, with the MEL-NPs group demonstrating more prominent recovery than the free MEL group. ZEA: zearalenone; MEL: melittin; MEL-NPs: melittin-loaded chitosan nanoparticles.

2.8. Histopathological Analysis of Ovarian Tissue

Histopathological examination was conducted to corroborate the biochemical findings of the present study. Ovarian sections from rats exposed to zearalenone (ZEA) revealed

distinct toxic alterations compared with the normal histoarchitecture of the control group. The ZEA-treated ovaries exhibited cystic degeneration of ovarian follicles, degeneration and vacuolation of corpora lutea cells, and a marked increase in interalveolar fibrosis, indicating severe structural and functional disruption. These findings were demonstrated through hematoxylin and eosin (H&E) staining of paraffin-embedded ovarian sections, examined and photographed at different magnifications (Low ×100 and High ×200) in the ovarian follicle (OF) and corpora lutea (CL) regions (Figure 7). Treatment with melittin (MEL) and melittin-loaded nanoparticles (MEL-NPs) markedly ameliorated the toxic histopathological changes induced by ZEA exposure, with MEL-NPs showing superior restoration of normal ovarian architecture compared to free MEL.

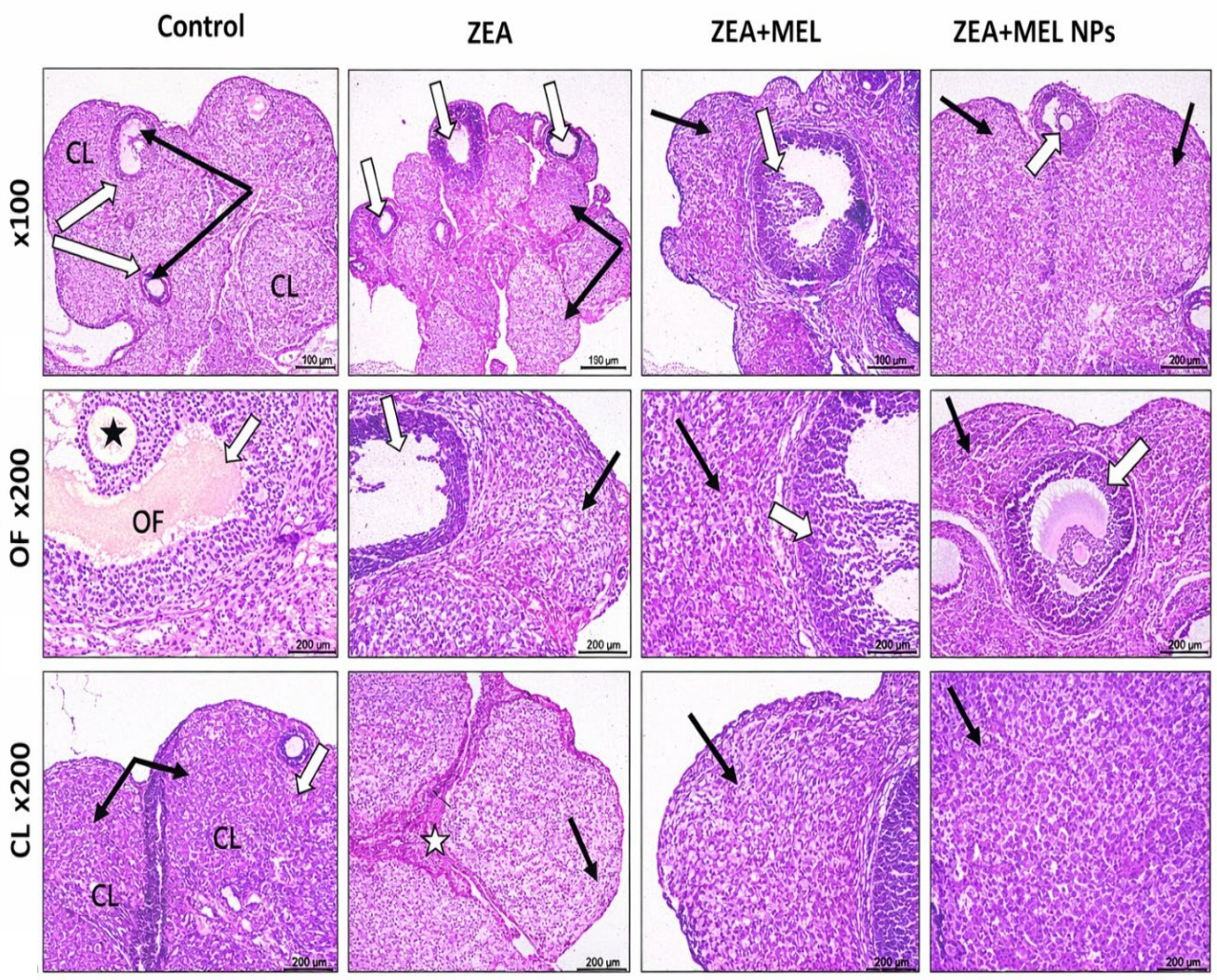


Figure 7. Representative histopathological images of the control and treatment groups' ovaries stained with H&E. Low ×100 and high ×200 magnification are used for the corpora lutea (CL) and ovarian follicles (OF) areas. The control group displayed corpora lutea (black arrows, CL) and several ovarian follicles (white arrows, OF) with undamaged ova (black star). Ovarian follicles with intact ova (white star) were absent from the ZEA group. Cystic alterations (white arrows) were seen in the others. Degenerative alterations in the corpora were characterized by increased intercorporate fibrosis (white star) and cellular vacuolation and loss of cellular characteristics (black arrows). ZEA + MEL group; group for therapy: Histological changes brought on by ZEA showed preservation, with corpora cells appearing less vacuolated (black arrows) and some immature follicles visible (white arrows). The ovarian tissue's natural structure, including the corpora (black arrows) and Graafian follicles (white arrows), was significantly restored in the ZEA + MEL NPs group and the nanotherapeutic group.

3. Discussion

Zearalenone (ZEA) is a potent estrogenic mycotoxin that has been widely studied for its ability to induce reproductive abnormalities in animals and hyperestrogenic syndromes in humans [27]. In addition to its reproductive toxicity, ZEA has been reported to exert systemic toxic effects on major metabolic organs, including the liver and kidneys [28]. Accordingly, the present study was designed to evaluate the protective and therapeutic potential of free melittin (MEL) and melittin-loaded chitosan nanoparticles (MEL-NPs) against ZEA-induced ovarian toxicity in female rats, with particular emphasis on oxidative stress, inflammation, apoptosis, and steroidogenic dysfunction.

ZEA exerts its toxic effects through multiple molecular mechanisms, primarily by mimicking estrogen and disrupting cellular redox homeostasis. ZEA and its metabolites competitively bind to estrogen receptors, leading to dysregulation of estrogen signaling and transcriptional activity in reproductive tissues. In parallel, ZEA promotes excessive generation of reactive oxygen species (ROS), suppresses antioxidant defenses, and induces DNA damage, cell-cycle arrest, and apoptosis through both intrinsic (mitochondrial) and extrinsic (death receptor–mediated) pathways [28,29]. Similar findings have been reported in porcine oocytes, where ZEA-induced toxicity was attenuated by activation of the PI3K/Akt pathway [30]. Collectively, these mechanisms contribute to ovarian injury, follicular atresia, and impaired reproductive function.

In the present work, melittin was successfully encapsulated within chitosan–TPP nanoparticles using the ionotropic gelation technique. Transmission electron microscopy confirmed the spherical morphology of MEL-NPs, with an average particle size of 37.5 nm, while a high encapsulation efficiency reached 94.12%, and an excellent loading capacity (LC) of 98.77%, indicating effective peptide loading. Fourier-transform infrared (FTIR) spectroscopy further verified the successful incorporation of melittin into the nanoparticle matrix. Shifts in the amide I and amide II bands, along with broadening of the O–H/N–H stretching region, indicated the formation of hydrogen bonding and electrostatic interactions between chitosan and melittin, consistent with previous reports on peptide-loaded chitosan nanoparticles [31,32]. These interactions suggest that melittin was structurally integrated within the chitosan–TPP network rather than superficially adsorbed, supporting nanoparticle stability and sustained peptide release.

Although nanoparticle morphology and size were verified using TEM and FT-IR spectroscopy, which confirmed successful melittin incorporation, additional characterization techniques such as dynamic light scattering (DLS) and zeta potential measurements would provide further information regarding particle size distribution, polydispersity index, and surface charge. These analyses were not available in the present study and represent an important aspect for future work.

Hormonal analysis revealed that ZEA exposure significantly increased serum luteinizing hormone (LH) and follicle-stimulating hormone (FSH) levels compared with the control group, indicating disruption of the hypothalamic–pituitary–ovarian axis. Such elevations are commonly associated with impaired ovarian feedback regulation and primary ovarian insufficiency [33]. Similar increases in LH and FSH following ZEA exposure have been reported by Collins et al. [34], whereas Milano et al. [35] observed no significant hormonal changes, highlighting dose- and model-dependent variability. Treatment with both free MEL and MEL-NPs attenuated these alterations, with MEL-NPs exerting a more pronounced regulatory effect, likely due to improved bioavailability and controlled release. Comparable hormonal modulation has been reported following bee venom administration [36], although context-dependent effects of melittin on LH release have also been described.

ZEA exposure resulted in a slight, nonsignificant increase in serum estradiol (E2) levels compared with controls. Previous studies have shown that ZEA may impair granulosa cell function and alter estrogen synthesis [27], although other investigations reported no significant changes in estradiol receptor expression following dietary ZEA exposure [37]. In the present study, neither free MEL nor MEL-NPs significantly altered E2 concentrations, indicating that the protective effects of melittin formulations were not mediated through direct modulation of estrogen synthesis.

In contrast, ZEA exposure markedly reduced serum progesterone levels, reflecting impaired luteal function and disrupted steroidogenesis. Progesterone deficiency is associated with abnormal estrous cyclicity, implantation failure, and reduced fertility [38,39]. Both free MEL and MEL-NPs significantly ameliorated the ZEA-induced decline in progesterone levels, with superior recovery observed in the MEL-NPs group. This improvement is most plausibly attributed to the antioxidant and anti-inflammatory actions of melittin nanoparticles, which preserve granulosa and luteal cell integrity and maintain steroidogenic enzyme activity.

At the molecular level, ZEA induced significant upregulation of pro-inflammatory cytokines, including TNF-α, IL-6, and IL-1β, confirming activation of ovarian inflammatory pathways. These findings are consistent with previous reports linking cytokine overproduction to granulosa cell injury and accelerated follicular atresia [40]. Concomitantly, ZEA markedly increased caspase-3 expression and activity, indicating activation of the apoptotic machinery and enhanced granulosa cell loss, in agreement with earlier studies describing caspase-mediated ovarian failure [41]. In addition, ZEA significantly downregulated CYP19A1 (aromatase), highlighting the vulnerability of ovarian steroidogenic pathways to oxidative and inflammatory insults [27,42].

Taken together, these findings support a mechanistic cascade in which ZEA-induced oxidative stress triggers inflammatory activation, promotes caspase-dependent apoptosis, and ultimately suppresses steroidogenic capacity, resulting in ovarian dysfunction, as proposed previously by Wu et al. (2025) [43].

Notably, treatment with MEL-NPs effectively counteracted these pathological changes. MEL-NPs significantly reduced pro-inflammatory cytokine expression, attenuated caspase-3 activation, restored antioxidant capacity, and partially normalized CYP19A1 expression. Although melittin has been reported to induce apoptosis in certain cancer cell models [44,45], its nanoformulated delivery in the present toxicant-injury context exerted a cytoprotective effect, consistent with previous reports on melittin nanoformulations. For instance, melittin nanoparticles have been shown to mitigate toxicant-induced organ injury by suppressing pro-inflammatory cytokines and enhancing antioxidant defenses [36]. Similarly, melittin exhibited anti-inflammatory and anti-apoptotic effects by downregulating TNF-α and IL-1β and inhibiting caspase-3 activation in vivo [46]. Moreover, melittin reduced inflammation and apoptosis in inflammatory cell models through modulation of cytokine expression and caspase pathways [47].

Although CYP19A1 plays a central role in ovarian estrogen biosynthesis through the conversion of androgens to estradiol, alterations in its gene expression do not always translate into parallel changes in circulating estradiol levels. In the present study, the downregulation of CYP19A1 expression following zearalenone exposure was not accompanied by a significant reduction in serum estradiol; several compensatory mechanisms may explain this. Previous studies have demonstrated that estrogen homeostasis can be maintained through extra-ovarian estrogen synthesis, particularly in adipose tissue and adrenal sources, which may partially compensate for reduced ovarian aromatase activity [48]. Additionally, estrogen regulation is highly tissue-specific, and local ovarian gene expression changes may not be immediately reflected in systemic hormone concentrations due to dynamic feed-

back regulation involving the hypothalamic–pituitary–gonadal axis [49]. Furthermore, the timing of sample collection represents a critical factor, as transient suppression of CYP19A1 expression may precede measurable hormonal alterations, particularly in short-term or subacute exposure models [25]. Importantly, inflammatory mediators such as TNF-α and IL-6 have been shown to suppress aromatase transcription without necessarily causing immediate changes in circulating estradiol, reinforcing the concept that CYP19A1 expression serves as a sensitive early molecular marker of steroidogenic disruption rather than a direct surrogate of serum estrogen levels [50]. Collectively, these findings support the interpretation that zearalenone-induced suppression of CYP19A1 reflects early steroidogenic impairment that may precede overt hormonal imbalance, and they further explain the apparent dissociation between gene expression and circulating estradiol levels observed in this study.

Biochemically, ZEA exposure significantly reduced total antioxidant capacity, reflecting oxidative stress and impaired redox balance [51,52]. Similar findings have been reported by Nguyen and Lee (2021) [53], whereas restoration of antioxidant defenses following bee venom or melittin treatment has been documented previously (e.g., melittin enhanced oxidant–antioxidant balance and upregulated antioxidant defenses in oxidative stress models).

In the present study, MEL-NPs markedly restored antioxidant levels compared with both the ZEA and free MEL groups, indicating superior efficacy in mitigating ROS-mediated damage.

In the current study, rats fed zearalenone (ZEA) for two weeks exhibited a significant increase in serum CA-125 levels compared with the control group. CA-125 is a glycoprotein expressed by various epithelial cells, particularly those of ovarian origin, and is widely recognized as a tumor biomarker for the diagnosis and monitoring of ovarian cancer [54]. Elevated CA-125 levels are not exclusive to ovarian malignancies; they may also be observed in cancers of the fallopian tubes, pancreas, breast, colorectum, lungs, and stomach [55]. Consistent with the findings of Minervini et al. [3], who reported that zearalenone exerts toxic effects on the female reproductive tract following acute exposure, our results suggest that the ZEA-induced elevation of CA-125 may reflect early pathological alterations or preneoplastic changes within ovarian or fallopian epithelial tissues. This elevation could therefore serve as an indicator of ZEA-related reproductive toxicity and potential tumorigenic risk. Treatment with free melittin (Free MEL) and melittin-loaded nanoparticles (MEL-NPs) markedly attenuated the ZEA-induced elevation in serum CA-125 levels. The MEL-NPs formulation demonstrated a greater reduction compared to the Free MEL group, reflecting its superior cytoprotective and anti-inflammatory potential. This enhanced effect is likely attributable to the improved physicochemical stability, controlled-release profile, and targeted delivery of melittin within the nanoparticle system, which collectively contribute to more efficient suppression of ZEA-induced oxidative stress and inflammatory pathways that drive epithelial injury and biomarker overexpression.

CA-125 was evaluated in the present study not as a cancer-specific marker, but as a potential indicator of ovarian epithelial and serosal stress or injury, since elevated serum CA-125 levels have been reported in a broad range of non-malignant conditions involving inflammation or tissue irritation, including endometriosis, uterine fibroids, pelvic inflammatory disease, and other serous effusions, beyond its traditional use in oncology diagnostics [56,57].

Morphological observations revealed visible differences in the uterine horns between groups. Rats in the ZEA group displayed inflammatory signs and fluid accumulation within the uterine lumen, likely reflecting estrogenic overstimulation and tissue edema. ZEA and its metabolites are known to bind to estrogen receptors (ERs), thereby disrupting ovarian activity and altering reproductive behavior in both animals and humans [5]. Due to its steroid-like structure, ZEA can also cause uterine edema, ovarian cyst formation, excessive follicular growth, and reduced fertilization rate, as previously reported in gilts [6].

Similar findings were observed in our study, where uterine horn distention and congestion were evident in the ZEA group.

Although morphological alterations of the uterus and ovaries were clearly observed, quantitative morphometric analysis, such as organ weight measurements or digital surface area analysis, was not performed in the present study. Future investigations incorporating morphometric quantification would provide additional objective evaluation of reproductive organ alterations induced by ZEA and their modulation by melittin nanoformulations.

Conversely, treatment with melittin and MEL-NPs alleviated these pathological changes, with MEL-NPs showing superior improvement compared to Free MEL. These results demonstrate that melittin nanoparticles can effectively preserve reproductive system integrity and protect against ZEA-induced reproductive toxicity. Histopathological examination of ovarian sections further supported these biochemical findings. The ZEA-treated group exhibited severe interstitial fibrosis, degeneration, and vacuolation of luteal cells, along with cystic follicular alterations. However, female rats treated with ZEA plus MEL-NPs showed marked structural restoration and minimal pathological alterations, consistent with the absence of gross morphological abnormalities. Collectively, these data confirm that MEL-NPs provide strong protection against ZEA-induced ovarian damage by restoring oxidative balance, reducing inflammation, and preventing apoptosis, ultimately maintaining normal reproductive histology and hormonal homeostasis.

Hormonal profiles and ovarian histology in rodents are strongly influenced by the stage of the estrous cycle. In the present study, estrous cycle staging was not monitored during the experimental period, which represents a limitation when interpreting endocrine outcomes. Although group randomization minimizes systematic bias, future studies incorporating vaginal cytology–based estrous cycle monitoring would allow for more precise assessment of hormone-dependent reproductive alterations.

Histopathological assessment in the present study was primarily qualitative. Quantitative histomorphometric approaches, including follicle counting at different developmental stages and assessment of follicular atresia rates, would provide additional objective insight into ovarian structural changes and will be incorporated in future studies.

One limitation of the present study is the absence of a nanoparticle-only control group (chitosan nanoparticles without melittin). Although chitosan nanoparticles are generally regarded as biocompatible and biologically inert carriers, inclusion of such a control would allow for clearer discrimination between the intrinsic biological effects of the carrier and the therapeutic activity of melittin.

In summary, the present findings demonstrate that ZEA-induced ovarian toxicity is mediated through an integrated inflammatory–apoptotic–steroidogenic axis. ZEA markedly increased ovarian TNF-α, IL-6, and IL-1β expression, consistent with previous reports linking ZEA exposure to ovarian inflammation and follicular damage [43]. This was accompanied by caspase-3 overexpression, supporting caspase-dependent apoptosis as a key mechanism of ZEA-induced ovarian injury [58]. Concurrent downregulation of CYP19A1 highlights disruption of steroidogenic capacity under inflammatory and oxidative stress conditions [59]. Importantly, melittin-loaded chitosan nanoparticles effectively reversed these molecular alterations by suppressing inflammation and apoptosis while restoring CYP19A1 expression, in agreement with recent evidence supporting the cytoprotective and anti-inflammatory potential of melittin nano-formulations [36].

4. Materials and Methods

4.1. Chemicals

Sigma Aldrich, Cairo, Egypt, supplied zearalenone (CAS No. 17924-92-4), melittin (CAS No. 20449-79-0), and sodium tripolyphosphate (CAS No. 7758-29-4). Chitosan, de-

rived from shrimp shells (*Pandalus borealis*), was purchased from Oxford Laboratory Chemicals, Mumbai, India, with low-molecular-weight chitosan (degree of deacetylation 93%).

4.2. Animals

Forty-eight mature female Wistar rats weighing 180–200 g and 10–12 weeks of age were supplied from the animal house at Sohag University in Sohag, Egypt. All of them were fed a balanced pellet meal and had unrestricted access to water in typical laboratory settings. Before the trial, the animals were acclimated to the laboratory environment and maintained in standard housing. Every ethical guideline was adhered to in accordance with the Institutional Animal Care and Use Committee, Faculty of Sciences, Sohag University, Sohag, Egypt, which provided ethical approval for this research, which was carried out by IACUC protocol no. SU-FS-5-26.

4.3. Study Design

After one week of acclimatization, forty-eight adult female Wistar rats were randomly allocated into four experimental groups (n = 12 animals per group) using a simple randomization procedure. The experimental groups were as follows:

Control group: Rats received the vehicle only (1% DMSO in saline) by oral gavage.

ZEA group: Rats received zearalenone at a dose of 2.7 mg/kg body weight administered orally twice weekly for two weeks to induce ovarian toxicity.

ZEA + MEL group: Rats were first exposed to zearalenone as described above, followed by treatment with free melittin (40 μg/kg body weight) administered orally three times per week for four weeks.

ZEA + MEL-NPs group: Rats were exposed to zearalenone and subsequently treated with melittin-loaded chitosan nanoparticles at an equivalent melittin dose (40 μg/kg body weight) administered orally three times per week for four weeks.

All treatments were administered by oral gavage using a sterile gastric tube. The dosing volume was adjusted to 1 mL per 100 g body weight. Zearalenone was dissolved in 1% DMSO in physiological saline, which was also used as the vehicle for the control group.

The experimental protocol was designed to evaluate the therapeutic efficacy of melittin and melittin-loaded chitosan nanoparticles against zearalenone-induced ovarian toxicity. The study was conducted in two sequential phases. In the first phase (weeks 1–2), ovarian toxicity was induced by oral administration of zearalenone at a dose of 2.7 mg/kg body weight twice weekly, as stated by EL-Sawi et al. [60]. In the second phase (weeks 3–6), animals received treatment with either free melittin or melittin-loaded chitosan nanoparticles at a dose of 40 μg/kg body weight administered orally three times per week, according to Abu-Zinadah et al. [61]. This experimental design for allowed for the assessment of the potential therapeutic effects of melittin formulations following toxin-induced ovarian injury.

The administered dose of melittin was maintained constant (40 μg/kg body weight) in both the free melittin (MEL) and melittin-loaded nanoparticle (MEL-NPs) groups to allow for direct comparison between the two formulations.

Throughout the experimental period, animals were monitored daily for signs of toxicity, including behavioral alterations, food and water intake, grooming behavior, and body weight changes. No mortality or visible adverse effects were observed in rats treated with either free melittin or melittin-loaded nanoparticles at the administered dose (40 μg/kg), indicating that the treatment regimen was well tolerated.

All treatments were administered according to the experimental grouping, and the duration of the study was six weeks. At the end of the experimental period, animals were sacrificed and ovarian tissues were collected for biochemical and molecular analyses. Blood samples from all groups were collected from the heart into plain tubes and centrifuged

at approximately 1800× *g* for 10 min to separate the serum. They were then divided into several aliquots and stored at −20 °C until analysis.

Ovarian Homogenate Preparation

Ovarian tissues were homogenized in cold potassium phosphate buffer (0.05 M, pH 7.4) using a glass homogenizer on ice to obtain a 10% (*w*/*v*) tissue homogenate. The homogenate was centrifuged at 5000× *g* for 10 min at 4 °C, and the resulting supernatant was collected and stored at −80 °C until biochemical analysis.

4.4. Preparation of Melittin-Loaded Chitosan–TPP Nanoparticles

Melittin-loaded chitosan nanoparticles were prepared using the ionic gelation method according to Walaa et al. [62]. Briefly, chitosan was dissolved in 1% (*v*/*v*) acetic acid to obtain a 0.2% (*w*/*v*) chitosan solution and adjusted to pH 5.5 using 1 M NaOH. Sodium tripolyphosphate (TPP) was dissolved in distilled water to obtain a 0.1% (*w*/*v*) solution. Melittin was dissolved in distilled water and added to the chitosan solution under continuous magnetic stirring. Subsequently, the TPP solution was added dropwise to the chitosan–melittin mixture under constant stirring at room temperature. The chitosan to TPP mass ratio was maintained at 5:1. The mixture was stirred for 30 min to allow for complete nanoparticle formation through electrostatic interaction between chitosan and TPP. The resulting nanoparticles were collected by centrifugation and washed with distilled water to remove unbound components. Finally, the nanoparticles formed were precipitated, dried at 70 °C for 24 h, and characterized.

Melittin-Loaded Chitosan–TPP Nanoparticles Characterization

The size and the surface morphology of MEL-NPs were observed by transmission electron microscopy (TEM) (JEOL JEM 1200 EXII, Microscope (JEOL Ltd., Tokyo, Japan)). TEM analysis was applied at NanoTech Company, Dokki, Egypt, according to Taher et al. [63].

CS, TPP, MEL, and MEL-loaded CS-NPs' FT-IR spectra were obtained by placing a small portion of the sample on the sensor of the Spectrophotometer (ATR-FTIR, Alpha Bruker Platinum, 1-211-6353, Bruker, Billerica, MA, USA) according to Devaraj et al. [64].

UV–vis absorption spectrum was obtained using a spectrophotometer (UviLine 9400, SECOMAM, Domont, France) at 280 nm to verify the formation of nanoparticles and evaluate the Loading Capacity of melittin nanoparticles according to Fakhari et al. [65].

The encapsulation efficiency (EE%) and loading capacity (LC%) of melittin in chitosan nanoparticles were determined to evaluate the drug entrapment and payload [66].

EE% was calculated using the following equation:

$$EE\% = \frac{Total\ drug\ added - Free\ drug}{Total\ drug\ added} \times 100$$

LC% was calculated using the equation:

$$LC\% = \frac{Total\ drug\ added - Free\ drug}{Total\ weight\ of\ nanoparticles} \times 100$$

where total drug added represents the initial amount of melittin used in the formulation, free drug is the unencapsulated melittin measured in the supernatant after centrifugation, and total weight of nanoparticles refers to the weight of the dried nanoparticles. The concentration of free melittin was quantified using UV–vis.

4.5. Biochemical Kits

An enzyme immunoassay test kit for quantitatively determining LH, FSH, E2, and the source of the serum's ovarian cancer antigen concentration was (BIOS Company, South San Francisco, CA 94080, USA). We purchased an enzyme immunoassay from PerkinElmer (Hayward, CA 94545, USA, Uok SA) to measure serum progesterone levels. TA 25 13 is the catalog number for the total antioxidant capacity kit for colorimetric determination in serum, which was purchased from Bio Diagnostic Company in Cairo, Egypt. An ELISA kit for the in vitro quantitative determination of Rat Caspase3 concentrations in serum was purchased from Elabscience Biotechnology Company (Catalog Number: E-EL-R0160, USA). TNF-α, IL-6, and IL-1β levels in ovarian tissue were measured using ELISA kits in accordance with the manufacturer's instructions. Catalog numbers E-EL-R0012 and E-EL-R0019, respectively, correspond to the TNF-α and IL-1β ELISA kits that were provided by Elabscience Biotechnology Inc. (Houston, TX, USA). We purchased the IL-6 ELISA kit from Invitrogen Fisher Scientific (Waltham, MA, USA) with catalog number LOT 192587043.

4.6. Quantitative Real-Time PCR (qRT-PCR)

Total RNA was extracted from tissue samples using TRIzol reagent following standard procedures. One microgram of RNA was reverse transcribed into cDNA using a commercial reverse transcription kit. Gene expression was quantified by qRT-PCR using SYBR Green chemistry (Applied Biosystems; Thermo Fisher Scientific, Inc., Waltham, MA, USA) on a Rotor-Gene Q system. Primers were designed for IL-1β, IL-6, TNF-α, Caspase 3, and CYP19A1, with GAPDH used as a housekeeping control (Table 1). Amplification conditions were optimized for each primer set, and all reactions were repeated five times. Relative gene expression levels were calculated using the $2^{-\Delta\Delta Ct}$ method, with the untreated control group serving as the reference. Primer specificity was confirmed by melt-curve analysis, and amplification efficiency ranged between 90 and 110 qRT-PCR reaction was performed in triplicate for at least $n = 5$ biological samples per group.

Each qRT-PCR reaction was performed in a final volume of 20 µL containing 10 µL SYBR Green Master Mix, 1 µL of forward primer, 1 µL of reverse primer, 2 µL of cDNA template, and 6 µL nuclease-free water. The thermal cycling conditions consisted of an initial denaturation at 95 °C for 5 min followed by 40 amplification cycles of denaturation at 95 °C for 15 s, annealing at the gene-specific temperature (Table 2) for 30 s, and extension at 72 °C for 30 s. Melt-curve analysis was performed to confirm amplification specificity.

Table 2. The qRT-PCR for each gene.

Genes	Primer Probes	Annealing Temperature	References
Caspase3	F:5′ CGGGGAGCTTGGAACGGTACG-3′ R:5′ TCCCAGAGTCCACTGACTTGC T-3′	60 °C	[67]
CYP19A1	F:5′-GCTGAACCCCATGCAGTA TAA-3′ R: 5′-AGCCAAAAGGCTGAAAGT ACC-3′	59 °C	[68]
IL-1β	F:5′-CTTTCCCGTGGACCTTCCA-3′ R:5′-CTCGGAGCCTGTAGTGCAGTT-3′	60 °C	[69]
IL-6	F:5′- TTGGTCCTTAGCCACTCCTTC-3′ R:5′-TAGTCCTTCCTACCCCAATTTCC-3′	60 °C	[70]
TNF-α	F: CCTATGTCTCAGCCTCTTCT-3′ R: CCTGGTATGAGATAGCAAAT-3′	58 °C	[71]
GAPDH	F:5′AGGAGTAAGAAACCCTGGAC-3′ R:5′-CTGGGATGGAATTGTGAG-3′	55 °C	[72]

4.7. Histopathological Examination

Ovarian tissues were fixed in 10% neutral buffered formalin for 24–48 h, dehydrated in graded ethanol series, cleared in xylene, and embedded in paraffin. Sections of approximately 5 µm thickness were cut using a microtome and mounted on glass slides. The sections were stained with hematoxylin and eosin (H&E) and examined under a light microscope for histopathological evaluation. Every technique was carried out in accordance with Suvarna et al. [73].

5. Statistical Analysis

Data was analyzed using the Statistical Package for the Social Sciences (SPSS version 26). The mean ± SE (standard error) was used to express the results. Tukey's contrast test was used to compare groups after one-way analysis of variance (ANOVA). A normal distribution with equal variance characterizes the values in each group. The significance levels were set at $p < 0.05$, $p < 0.01$, and $p < 0.001$.

For biochemical and hormonal assays, analyses were performed using serum samples from at least six animals per group (biological replicates). Each measurement was performed in duplicate technical replicates.

6. Conclusions

Zearalenone (ZEA) induced severe ovarian toxicity via oxidative stress, inflammation, apoptosis, and disruption of steroidogenesis, resulting in significant biochemical, hormonal, and histopathological alterations with impaired ovarian structure and function. Both free melittin (MEL) and melittin-loaded chitosan nanoparticles (MEL-NPs) ameliorated ZEA-induced ovarian damage; however, MEL-NPs demonstrated superior efficacy. The nanoformulation more effectively restored antioxidant balance, suppressed pro-inflammatory cytokines, inhibited caspase-3–mediated apoptosis, and enhanced steroidogenic function through upregulation of CYP19A1, thereby preserving follicular integrity and ovarian architecture.

These results suggest that chitosan-based nanoparticle delivery improves melittin bioavailability and enhances its protective potential against mycotoxin-induced ovarian dysfunction. MEL-NPs represent a promising nanotherapeutic strategy, yet further studies in higher mammalian models, along with detailed pharmacokinetic, toxicity, and long-term reproductive safety evaluations, are warranted.

Author Contributions: R.A.R., A.M.H. and N.S.M. conceived and designed the study. R.A.R., A.M.H., S.N.M.F., Z.E.E.M. and E.E.M.H. performed the experimental work and sample collection. A.M.H., A.M.R. and R.M.I. conducted the blood biochemical assays and tumor marker analyses. A.M.H. was responsible for the preparation, characterization, and data analysis of melittin-loaded chitosan–TPP nanoparticles. N.A.R.F. performed the histopathological examination of ovarian tissues and interpreted the histological findings. N.M.E.-S. and G.S.M. contributed to data curation and statistical analysis. E.K.N. assisted in laboratory work and data organization. P.E.M. contributed to methodology optimization and critical scientific revision of the manuscript. R.A.R. and A.M.H. drafted the manuscript. A.M.R., N.A.R.F., N.M.E.-S. and N.S.M. contributed to manuscript writing, editing, and critical revision. All authors have read and agreed to the published version of the manuscript.

Funding: This research received no external funding.

Institutional Review Board Statement: The study received ethical approval from the Institutional Animal Care and Use Committee (IACUC), Faculty of Science, Sohag University, Sohag, Egypt, under protocol number SU-FS-5-26 (approval date: 1 February 2026).

Informed Consent Statement: Not applicable.

Data Availability Statement: All data generated or analyzed during this study are included in this published article.

Conflicts of Interest: The authors reported no potential conflicts of interest.

Abbreviations

ZEA: Zearalenone; MEL: Melittin; Cs-NPs: Chitosan Nanoparticles; TPP: Tripolyphosphate; UV-Vis: Ultraviolet–Visible Spectroscopy; FT-IR: Fourier-Transform Infrared; TEM: Transmission Electron Microscopy; LC: Loading Capacity; BV: Bee venom; CA: Cancer Antigen; E2: Estradiol; FSH: Follicle Stimulating Hormone; LH: Luteinizing Hormone; TAC: Total Antioxidant Capacity; H&E stain: Hematoxylin & Eosin stain; OF: Ovarian Follicles; CL: Corpora Lutea; ROS: Reactive Oxygen Species.

References

1. Alshannaq, A.; Yu, J.-H. Occurrence, toxicity, and analysis of major mycotoxins in food. *Int. J. Environ. Res. Public Health* **2017**, *14*, 632. [CrossRef]
2. El Sawi, N.M.; Muhammad Marie, O.; Shaker Ali, S.; Hamed, A. Toxicity Assessment of Zearalenone in Ovarian Female Rats. *Sohag J. Sci.* **2022**, *7*, 161–165. [CrossRef]
3. Minervini, F.; Dell'Aquila, M.; Maritato, F.; Minoia, P.; Visconti, A. Toxic effects of the mycotoxin zearalenone and its derivatives on in vitro maturation of bovine oocytes and 17β-estradiol levels in mural granulosa cell cultures. *Toxicol. In Vitro* **2001**, *15*, 489–495. [CrossRef] [PubMed]
4. Abbasian, N.; Momtaz, S.; Baeeri, M.; Navaei-Nigjeh, M.; Hosseini, R.; Abdollahi, M. Molecular and biochemical evidence on the role of zearalenone in rat polycystic ovary. *Toxicon* **2018**, *154*, 7–14. [CrossRef] [PubMed]
5. Jakimiuk, E.; Kuciel-Lisiecka, G.; Zwierzchowski, W.; Gajęcka, M.; Obremski, K.; Zielonka, Ł.; Skorska-Wyszyńska, E.; Gajęcki, M. Morphometric changes of the reproductive system in gilts during zearalenone mycotoxicosis. *Med. Weter.* **2006**, *62*, 99–102.
6. Minervini, F.; Dell'Aquila, M.E. Zearalenone and reproductive function in farm animals. *Int. J. Mol. Sci.* **2008**, *9*, 2570–2584. [CrossRef]
7. Jeong, Y.-J.; Choi, Y.; Shin, J.-M.; Cho, H.-J.; Kang, J.-H.; Park, K.-K.; Choe, J.-Y.; Bae, Y.-S.; Han, S.-M.; Kim, C.-H. Melittin suppresses EGF-induced cell motility and invasion by inhibiting PI3K/Akt/mTOR signaling pathway in breast cancer cells. *Food Chem. Toxicol.* **2014**, *68*, 218–225. [CrossRef]
8. Kohno, M.; Horibe, T.; Ohara, K.; Ito, S.; Kawakami, K. The membrane-lytic peptides K8L9 and melittin enter cancer cells via receptor endocytosis following subcytotoxic exposure. *Chem. Biol.* **2014**, *21*, 1522–1532. [CrossRef]
9. Mahmoodzadeh, A.; Morady, A.; Zarrinnahad, H.; Pooshang Bagheri, K.; Ghasemi-Dehkordi, P.; Mahdavi, M.; Shahbazzadeh, D.; Shahmorady, H. Isolation of melittin from bee venom and evaluation of its effect on proliferation of gastric cancer cells. *Tehran Univ. Med. J.* **2013**, *70*, 26–32.
10. Mahmoodzadeh, A.; Zarrinnahad, H.; Bagheri, K.P.; Moradia, A.; Shahbazzadeh, D. First report on the isolation of melittin from Iranian honey bee venom and evaluation of its toxicity on gastric cancer AGS cells. *J. Chin. Med. Assoc.* **2015**, *78*, 574–583. [CrossRef]
11. Liu, M.; Zong, J.; Liu, Z.; Li, L.; Zheng, X.; Wang, B.; Sun, G. A novel melittin-MhIL-2 fusion protein inhibits the growth of human ovarian cancer SKOV 3 cells in vitro and in vivo tumor growth. *Cancer Immunol. Immunother.* **2013**, *62*, 889–895. [CrossRef]
12. Qian, C.-Y.; Wang, K.-L.; Fang, F.-F.; Gu, W.; Huang, F.; Wang, F.-Z.; Li, B.; Wang, L.-N. Triple-controlled oncolytic adenovirus expressing melittin to exert inhibitory efficacy on hepatocellular carcinoma. *Int. J. Clin. Exp. Pathol.* **2015**, *8*, 10403.
13. Shin, J.-M.; Jeong, Y.-J.; Cho, H.-J.; Park, K.-K.; Chung, I.-K.; Lee, I.-K.; Kwak, J.-Y.; Chang, H.-W.; Kim, C.-H.; Moon, S.-K. Melittin suppresses HIF-1α/VEGF expression through inhibition of ERK and mTOR/p70S6K pathway in human cervical carcinoma cells. *PLoS ONE* **2013**, *8*, e69380. [CrossRef] [PubMed]
14. Jo, M.; Park, M.H.; Kollipara, P.S.; An, B.J.; Song, H.S.; Han, S.B.; Kim, J.H.; Song, M.J.; Hong, J.T. Anti-cancer effect of bee venom toxin and melittin in ovarian cancer cells through induction of death receptors and inhibition of JAK2/STAT3 pathway. *Toxicol. Appl. Pharmacol.* **2012**, *258*, 72–81. [CrossRef] [PubMed]
15. Bhattarai, N.; Ramay, H.R.; Chou, S.-H.; Zhang, M. Chitosan and lactic acid-grafted chitosan nanoparticles as carriers for prolonged drug delivery. *Int. J. Nanomed.* **2006**, *1*, 181. [CrossRef]
16. Dustgania, A.; Vasheghani Farahani, E.; Imani, M. Preparation of chitosan nanoparticles loaded by dexamethasone sodium phosphate. *Iran. J. Pharm. Sci.* **2008**, *4*, 111–114.
17. Tiyaboonchai, W. Chitosan nanoparticles: A promising system for drug delivery. *Naresuan Univ. J. Sci. Technol. (NUJST)* **2013**, *11*, 51–66.

18. Shahbazi, M.A.; Hamidi, M.; Peymani, P. Interaction of chitosan, a natural polymer used in Nanodrug/gene delivery, with non-steroidal anti-inflammatory drugs (NSAIDs). *Internet J. Nanotechnol.* **2008**, *2*, 1–7.
19. Singh, R.; Shitiz, K.; Singh, A. Chitin and chitosan: Biopolymers for wound management. *Int. Wound J.* **2017**, *14*, 1276–1289. [CrossRef]
20. Aranaz, I.; Alcántara, A.R.; Civera, M.C.; Arias, C.; Elorza, B.; Heras Caballero, A.; Acosta, N. Chitosan: An Overview of Its Properties and Applications. *Polymers* **2021**, *13*, 3256. [CrossRef]
21. Honarkar, H.; Barikani, M. Applications of biopolymers I: Chitosan. *Monatsh. Chem.-Chem. Mon.* **2009**, *140*, 1403–1420. [CrossRef]
22. Pan, Y.; Li, Y.-J.; Zhao, H.-Y.; Zheng, J.-M.; Xu, H.; Wei, G.; Hao, J.-S. Bioadhesive polysaccharide in protein delivery system: Chitosan nanoparticles improve the intestinal absorption of insulin in vivo. *Int. J. Pharm.* **2002**, *249*, 139–147. [CrossRef] [PubMed]
23. Yi, Y.; Wan, S.; Wang, S.; Khan, A.; Guo, J.; Zheng, X.; Li, H.; Sun, N. Scutellarin protects mouse ovarian granulosa cells from injury induced by the toxin zearalenone. *Food Funct.* **2021**, *12*, 1252–1261. [CrossRef] [PubMed]
24. Li, Y.; Gao, Y.; Yao, D.; Li, Z.; Wang, J.; Zhang, X.; Zhao, X.; Zhang, Y. Heme Oxygenase-1 Regulates Zearalenone-Induced Oxidative Stress and Apoptosis in Sheep Follicular Granulosa Cells. *Int. J. Mol. Sci.* **2024**, *25*, 2578. [CrossRef] [PubMed]
25. Wan, B.; Yuan, X.; Yang, W.; Jiao, N.; Li, Y.; Liu, F.; Liu, M.; Yang, Z.; Huang, L.; Jiang, S. The Effects of Zearalenone on the Localization and Expression of Reproductive Hormones in the Ovaries of Weaned Gilts. *Toxins* **2021**, *13*, 626. [CrossRef]
26. Lv, Q.; Xu, W.; Yang, F.; Wei, W.; Chen, X.; Zhang, Z.; Liu, Y. Reproductive Toxicity of Zearalenone and Its Molecular Mechanisms: A Review. *Molecules* **2025**, *30*, 505. [CrossRef]
27. Balló, A.; Busznyákné Székvári, K.; Czétány, P.; Márk, L.; Török, A.; Szántó, Á.; Máté, G. Estrogenic and non-estrogenic disruptor effect of zearalenone on male reproduction: A review. *Int. J. Mol. Sci.* **2023**, *24*, 1578. [CrossRef]
28. Xia, J.; Wan, Y.; Wu, J.-j.; Yang, Y.; Xu, J.-F.; Zhang, L.; Liu, D.; Chen, L.; Tang, F.; Ao, H. Therapeutic potential of dietary flavonoid hyperoside against non-communicable diseases: Targeting underlying properties of diseases. *Crit. Rev. Food Sci. Nutr.* **2024**, *64*, 1340–1370. [CrossRef]
29. Zheng, W.; Wang, B.; Li, X.; Wang, T.; Zou, H.; Gu, J.; Yuan, Y.; Liu, X.; Bai, J.; Bian, J. Zearalenone promotes cell proliferation or causes cell death? *Toxins* **2018**, *10*, 184. [CrossRef]
30. Li, X.; Duan, J.; Wang, S.; Cheng, J.; Chen, H.; Zhang, Z.; Yang, L.; Hua, R.; Li, Q. Isorhamnetin protects porcine oocytes from zearalenone-induced reproductive toxicity through the PI3K/Akt signaling pathway. *J. Anim. Sci. Biotechnol.* **2023**, *14*, 22. [CrossRef]
31. Pudžaitis, V. Surface Enhanced Infrared Absorption Spectroscopy of Biomolecular Layers and Water at Gold Surface. Ph.D. Thesis, Vilniaus Universitetas, Vilnius, Lithuania, 2024.
32. Lott, L.Q. Chitosan Surface Functionalized Nanodiamonds for Enhanced Drug Delivery. Ph.D. Thesis, Delaware State University, Dover, DE, USA, 2021.
33. Wu, F.; Cui, J.; Yang, X.; Chen, B. Effects of zearalenone on vulva area, liver function, serum immunoglobulin, antioxidant capability and sex hormone secretion of prepubertal gilts. *Ital. J. Anim. Sci.* **2022**, *21*, 1604–1610. [CrossRef]
34. Collins, T.F.; Sprando, R.L.; Black, T.N.; Olejnik, N.; Eppley, R.M.; Alam, H.Z.; Rorie, J.; Ruggles, D.I. Effects of zearalenone on in utero development in rats. *Food Chem. Toxicol.* **2006**, *44*, 1455–1465. [CrossRef] [PubMed]
35. Milano, G.D.; Becú-Villalobos, D.; Tapia, M.O. Effects of long-term zearalenone administration on spermatogenesis and serum luteinizing hormone, follicle-stimulating hormone, and prolactin values in male rats. *Am. J. Vet. Res.* **1995**, *56*, 954–958. [CrossRef] [PubMed]
36. Hamed, A.M.; Eldeeb Mohana, Z.E.; Abouelella, A.M.; Abdellah, W.A.; Elbahy, D.A.; Fouda, N.A.; Monir, D.M.; Soliman, S.S.; Mahmoud Abdelfattah Elkassas, A.M.; Hamouda, E.E.M. Melittin Nanoparticles Mitigate Glyphosate-Induced Nephrotoxicity via Cytokine Modulation and Bax/Nrf2 Pathways. *Biomedicines* **2025**, *13*, 2607. [CrossRef] [PubMed]
37. Gajęcka, M.; Otrocka-Domagała, I.; Brzuzan, P.; Dąbrowski, M.; Lisieska-Żołnierczyk, S.; Zielonka, Ł.; Gajęcki, M.T. Immunohistochemical Expression (IE) of Oestrogen Receptors in the Intestines of Prepubertal Gilts Exposed to Zearalenone. *Toxins* **2023**, *15*, 122. [CrossRef]
38. Wyse, J.; Latif, S.; Gurusinghe, S.; McCormick, J.; Weston, L.A.; Stephen, C.P. Phytoestrogens: A review of their impacts on reproductive physiology and other effects upon grazing livestock. *Animals* **2022**, *12*, 2709. [CrossRef]
39. Song, T.; Zhou, X.; Ma, X.; Jiang, Y.; Yang, W.; Liu, F.; Liu, M.; Huang, L.; Jiang, S. Zearalenone Promotes Uterine Development of Weaned Gilts by Interfering with Serum Hormones and Up-Regulating Expression of Estrogen and Progesterone Receptors. *Toxins* **2022**, *14*, 732. [CrossRef]
40. Rajendran, P.; Ammar, R.B.; Al-Saeedi, F.J.; Mohamed, M.E.; ElNaggar, M.A.; Al-Ramadan, S.Y.; Bekhet, G.M.; Soliman, A.M. Kaempferol inhibits zearalenone-induced oxidative stress and apoptosis via the PI3K/Akt-mediated Nrf2 signaling pathway: In vitro and in vivo studies. *Int. J. Mol. Sci.* **2020**, *22*, 217. [CrossRef]
41. Li, X.; Chen, H.; Zhang, Z.; Duan, J.; Hua, R.; Li, X.; Yang, L.; Cheng, J.; Li, Q. Isorhamnetin protects zearalenone-induced damage via the PI3K/Akt signaling pathway in porcine ovarian granulosa cells. *Anim. Nutr.* **2022**, *11*, 381–390. [CrossRef]

42. Zhang, G.-L.; Zhang, R.-Q.; Sun, X.-F.; Cheng, S.-F.; Wang, Y.-F.; Ji, C.-L.; Feng, Y.-Z.; Yu, J.; Ge, W.; Zhao, Y. RNA-seq based gene expression analysis of ovarian granulosa cells exposed to zearalenone in vitro: Significance to steroidogenesis. *Oncotarget* **2017**, *8*, 64001. [CrossRef]
43. Wu, F.; Wang, F.; Tang, Z.; Yang, X.; Liu, Y.; Zhao, M.; Liu, S.; Han, S.; Chen, B. Zearalenone causes ovarian damage and abnormal estradiol secretion in meat rabbits by inducing oxidative stress and inflammatory responses. *Front. Vet. Sci.* **2025**, *12*, 1566284. [CrossRef]
44. Haque, S.; Hussain, A.; Joshi, H.; Sharma, U.; Sharma, B.; Aggarwal, D.; Rani, I.; Ramniwas, S.; Gupta, M.; Tuli, H.S. Melittin: A possible regulator of cancer proliferation in preclinical cell culture and animal models. *J. Cancer Res. Clin. Oncol.* **2023**, *149*, 17709–17726. [CrossRef] [PubMed]
45. Kong, G.-M.; Tao, W.-H.; Diao, Y.-L.; Fang, P.-H.; Wang, J.-J.; Bo, P.; Qian, F. Melittin induces human gastric cancer cell apoptosis via activation of mitochondrial pathway. *World J. Gastroenterol.* **2016**, *22*, 3186. [CrossRef] [PubMed]
46. Park, J.-H.; Kim, K.-H.; Lee, W.-R.; Han, S.-M.; Park, K.-K. Protective effect of melittin on inflammation and apoptosis in acute liver failure. *Apoptosis* **2012**, *17*, 61–69. [CrossRef] [PubMed]
47. Lee, W.-R.; Kim, K.-H.; An, H.-J.; Kim, J.-Y.; Han, S.-M.; Lee, K.-G.; Park, K.-K. Protective effect of melittin against inflammation and apoptosis on Propionibacterium acnes-induced human THP-1 monocytic cell. *Eur. J. Pharmacol.* **2014**, *740*, 218–226. [CrossRef]
48. Collin, P.; Kaukinen, K.; Välimäki, M.; Salmi, J. Endocrinological Disorders and Celiac Disease. *Endocr. Rev.* **2002**, *23*, 464–483. [CrossRef]
49. Christian, C.A.; Moenter, S.M. The Neurobiology of Preovulatory and Estradiol-Induced Gonadotropin-Releasing Hormone Surges. *Endocr. Rev.* **2010**, *31*, 544–577. [CrossRef]
50. Bartkowiak-Wieczorek, J.; Jaros, A.; Gajdzińska, A.; Wojtyła-Buciora, P.; Szymański, I.; Szymaniak, J.; Janusz, W.; Walczak, I.; Jonaszka, G.; Bienert, A. The dual faces of oestrogen: The impact of exogenous oestrogen on the physiological and pathophysiological functions of tissues and organs. *Int. J. Mol. Sci.* **2024**, *25*, 8167. [CrossRef]
51. Tatay, E.; Espin, S.; Garcia-Fernandez, A.-J.; Ruiz, M.-J. Oxidative damage and disturbance of antioxidant capacity by zearalenone and its metabolites in human cells. *Toxicol. In Vitro* **2017**, *45*, 334–339. [CrossRef]
52. Salem, I.B.; Boussabbeh, M.; Neffati, F.; Najjar, M.; Abid-Essefi, S.; Bacha, H. Zearalenone-induced changes in biochemical parameters, oxidative stress and apoptosis in cardiac tissue: Protective role of crocin. *Hum. Exp. Toxicol.* **2016**, *35*, 623–634. [CrossRef]
53. Nguyen, C.D.; Lee, G. Neuroprotective Activity of Melittin-The Main Component of Bee Venom-Against Oxidative Stress Induced by Aβ(25-35) in In Vitro and In Vivo Models. *Antioxidants* **2021**, *10*, 1654. [CrossRef]
54. Rao, S.; Smith, D.A.; Guler, E.; Kikano, E.G.; Rajdev, M.A.; Yoest, J.M.; Ramaiya, N.H.; Tirumani, S.H. Past, Present, and Future of Serum Tumor Markers in Management of Ovarian Cancer: A Guide for the Radiologist. *RadioGraphics* **2021**, *41*, 1839–1856. [CrossRef] [PubMed]
55. Nossov, V.; Amneus, M.; Su, F.; Lang, J.; Janco, J.M.T.; Reddy, S.T.; Farias-Eisner, R. The early detection of ovarian cancer: From traditional methods to proteomics. Can we really do better than serum CA-125? *Am. J. Obstet. Gynecol.* **2008**, *199*, 215–223. [CrossRef] [PubMed]
56. Bălăceanu, L.A.; Grigore, C.; Dina, I.; Gurău, C.D.; Mihai, M.M.; Bălăceanu-Gurău, B. CA125 as a Potential Biomarker in Non-Malignant Serous Effusions: Diagnostic and Prognostic Considerations. *J. Clin. Med.* **2025**, *14*, 4152. [CrossRef] [PubMed]
57. Dochez, V.; Caillon, H.; Vaucel, E.; Dimet, J.; Winer, N.; Ducarme, G. Biomarkers and algorithms for diagnosis of ovarian cancer: CA125, HE4, RMI and ROMA, a review. *J. Ovarian Res.* **2019**, *12*, 28. [CrossRef]
58. Zhu, Y.; Wang, H.; Wang, J.; Han, S.; Zhang, Y.; Ma, M.; Zhu, Q.; Zhang, K.; Yin, H. Zearalenone Induces Apoptosis and Cytoprotective Autophagy in Chicken Granulosa Cells by PI3K-AKT-mTOR and MAPK Signaling Pathways. *Toxins* **2021**, *13*, 199. [CrossRef]
59. Han, X.; Huangfu, B.; Xu, T.; Xu, W.; Asakiya, C.; Huang, K.; He, X. Research Progress of Safety of Zearalenone: A Review. *Toxins* **2022**, *14*, 386. [CrossRef]
60. EL-Sawi, N.M.; Al-Seeni, M.N.; Younes, S.H.; AL-Jahdali, S.M.; Ali, S.S. Biochemical and histological studies on the effect of zearalenone mycotoxin and thymoquinone on male mice kidney. *J. Am. Sci.* **2012**, *8*, 378–388.
61. Abu-Zinadah, O.; Rahmy, T.; Alahmari, A.; Abdu, F. Effect of melittin on mice stomach. *Saudi J. Biol. Sci.* **2014**, *21*, 99–108. [CrossRef]
62. Walaa, A.M.; Samia, E.; Fatma, A.T.; Aly, F.M.; Karima, M. Evaluation of anticancer potentials of bee free venom and chitosan nano-conjugated one: In vitro study. *Int. J. Sci. Res. Manag.* **2017**, *5*, 5253–5262.
63. Taher, F.; Moselhy, W.; Mohamed, A.; Didamony, S.; Metwalley, K.; Zayed, A. Preparation and characterization of shrimp derived chitosan and evaluation of its efficiency as bee venom delivery for cancer treatment. *Int. J. Adv. Res.* **2017**, *5*, 370–388. [CrossRef]
64. Devaraj, P.; Kumari, P.; Aarti, C.; Renganathan, A. Synthesis and characterization of silver nanoparticles using cannonball leaves and their cytotoxic activity against MCF-7 cell line. *J. Nanotechnol.* **2013**, *2013*, 598328. [CrossRef]

65. Fakhari, S.; Jamzad, M.; Kabiri Fard, H. Green synthesis of zinc oxide nanoparticles: A comparison. *Green Chem. Lett. Rev.* **2019**, *12*, 19–24. [CrossRef]
66. Mohammadpour Dounighi, N.; Eskandari, R.; Avadi, M.R.; Zolfagharian, H.; Mir Mohammad Sadeghi, A.; Rezayat, M. Preparation and in vitro characterization of chitosan nanoparticles containing Mesobuthus eupeus scorpion venom as an antigen delivery system. *J. Venom. Anim. Toxins Incl. Trop. Dis.* **2012**, *18*, 44–52. [CrossRef]
67. Balogh, B.; Szarka, G.; Tengölics, Á.J.; Hoffmann, G.; Völgyi, B.; Kovács-Öller, T. LED-induced microglial activation and rise in caspase3 suggest a reorganization in the retina. *Int. J. Mol. Sci.* **2021**, *22*, 10418. [CrossRef]
68. Wong, S.; Tan, K.; Carey, K.T.; Fukushima, A.; Tiganis, T.; Cole, T.J. Glucocorticoids stimulate hepatic and renal catecholamine inactivation by direct rapid induction of the dopamine sulfotransferase Sult1d1. *Endocrinology* **2010**, *151*, 185–194. [CrossRef]
69. Yang, L.; Zhang, S.; Duan, H.; Dong, M.; Hu, X.; Zhang, Z.; Wang, Y.; Zhang, X.; Shi, W.; Zhou, Q. Different effects of pro-inflammatory factors and hyperosmotic stress on corneal epithelial stem/progenitor cells and wound healing in mice. *Stem Cells Transl. Med.* **2019**, *8*, 46–57. [CrossRef]
70. Dong, W.; Embury, C.M.; Lu, Y.; Whitmire, S.M.; Dyavarshetty, B.; Gelbard, H.A.; Gendelman, H.E.; Kiyota, T. The mixed-lineage kinase 3 inhibitor URMC-099 facilitates microglial amyloid-β degradation. *J. Neuroinflamm.* **2016**, *13*, 184. [CrossRef]
71. Lee, E.-J.; Ko, H.-M.; Jeong, Y.-H.; Park, E.-M.; Kim, H.-S. β-Lapachone suppresses neuroinflammation by modulating the expression of cytokines and matrix metalloproteinases in activated microglia. *J. Neuroinflamm.* **2015**, *12*, 133. [CrossRef]
72. Li, Y.-J.; Zhu, P.; Liang, Y.; Yin, W.-G.; Xiao, J.-H. Hepatitis B virus induces expression of cholesterol metabolism-related genes via TLR2 in HepG2 cells. *World J. Gastroenterol.* **2013**, *19*, 2262.
73. Suvarna, K.S.; Layton, C.; Bancroft, J.D. *Bancroft's Theory and Practice of Histological Techniques E-Book*; Elsevier Health Sciences: Amsterdam, The Netherlands, 2018.

Disclaimer/Publisher's Note: The statements, opinions and data contained in all publications are solely those of the individual author(s) and contributor(s) and not of MDPI and/or the editor(s). MDPI and/or the editor(s) disclaim responsibility for any injury to people or property resulting from any ideas, methods, instructions or products referred to in the content.